Far Infrared Observations of the Galactic Star Forming Regions associated with IRAS 00338+6312 & RAFGL 5111

B. Mookerjea 1, S.K. Ghosh 1, A.D. Karnik 1, T.N. Rengarajan 1,

S.N. Tandon 2 & R.P. Verma¹

Received ____

accepted _

¹Tata Institute of Fundamental Research, Homi Bhabha Road, Mumbai 400 005, India ²Inter-University Centre for Astronomy & Astrophysics, Ganeshkhind, Pune 411 007, India

ABSTRACT

Two Galactic star forming regions, one in a very early phase of evolution and another evolved one, associated with the IRAS sources 00338+6312 and 03595+5110 (RAFGL 5111) respectively have been studied in detail. These sources have been mapped simultaneously in two far infrared bands ($\lambda_{\text{eff}} = 143$ & 185 µm), with ~ 1'.5 angular resolution, using the TIFR 100 cm balloon borne telescope. The HIRES processed IRAS maps at 12, 25, 60 & 100 µm, have been used for comparison. Whereas IRAS 00338+6312 is resolved only in the TIFR bands, RAFGL 5111 is very well resolved in both the TIFR bands, as well as in at least 3 IRAS bands. The neighbouring fainter source IRAS 04004+5114 has also been resolved in the TIFR bands. Taking advantage of the identical beams in the two TIFR bands at 143 & 185 µm, dust colour temperature, T(143/185), and optical depth, τ_{150} , maps have been generated for RAFGL 5111. These maps show interesting structural details.

Radiative transfer modelling in spherical geometry has been carried out for individual sources to extract information about: the cloud size, type of the embedded source, radial density distribution, optical depth, gas to dust ratio, and the dust grain composition. The best fit models are in good agreement with the observed spectral energy distribution (SED), radio continuum data etc. Another scheme of radiative transfer through the interstellar dust-gas cloud including the heavier elements has been used to predict ionic nebular line emission, which are in reasonable agreement with the measurements for RAFGL 5111. An important conclusion from the present study is that, for all the three sources (IRAS 00338+6312; 03595+5110; and 04004+5114, a faint source in the neighbourhood of RAFGL 5111), the best fit to the observed SED is obtained for a uniform density $(n(r) \sim r^0)$ cloud. Subject Headings: IRAS 00338+6312 – RAFGL 5111 – IRAS 03595+5110 – IRAS 04004+5114 – Far Infrared Mapping – Radiative Transfer – H II region

1. Introduction

In order to get complete information and understanding of the energetics, physical sizes, spatial distribution of interstellar dust, and the role of the cooler (< 20 K) dust in Galactic star forming regions, high angular resolution mapping in trans-IRAS wavebands ($\lambda_{eff} > 100 \mu$ m) is essential. With the above in view, a programme of high angular resolution mapping of Galactic star forming regions in far infrared (FIR) bands using the TIFR 100 cm balloon borne telescope, was undertaken. At present a two band FIR photometer, with effective wavelengths of 143 μ m and 185 μ m is in regular use. This photometer uses bolometer arrays thereby resulting in much higher observational efficiency (Verma, Rengarajan & Ghosh 1993). Several individual Galactic star forming regions have been observed in a series of balloon flights during 1993-98 (Ghosh et al. 1996, Karnik et al. 1999, Mookerjea et al. 1999). The present paper deals with the two star forming regions associated with IRAS 00338+6312 and 03595+5110 (RAFGL 5111).

IRAS 00338+6312 is an unidentified IRAS Point Source Catalog (hereafter IRAS PSC) source with its spectrum rising steeply from 25 to 60 to 100 μ m, typical of YSO's. It is located near the core of the dark cloud L1287. A near-IR survey of Herbig-Haro objects and candidates (with red nebulosity) led Persi et al. (1988) to suggest that RNO 1 may be identified with IRAS 00338+6312. Snell, Dickman & Huang (1990) discovered an energetic molecular outflow activity in IRAS 00338+6312 from their ¹²CO measurements. Further millimeter wave line studies in CO, HCN and HCO⁺ by Yang et al. (1991) confirmed the outflow activity. They identified the driving source for the outflow to be IRAS 00338+6312.

With the discovery of a new FU Orionis type source, RNO 1B (which brightened by over 3 magnitudes since 1978), right inside the IRAS positional error ellipse, Staude & Neckel (1991) suggested that the energetic outflow is powered by FU Ori activity. This was supported by the discovery of a second FU Orionis source RNO 1C (Kenyon et al. 1993);

& CS line and mm-wave continuum study of the FU Ori binary system RNO 1B/1C, by McMuldroch, Blake & Sargent (1995).

The resolution to the debate between whether the outflow activity is powered by a deeply embedded YSO or FU Ori activity, came from the following clinching evidences : (i) high spatial resolution (0.1'') near-IR $(3.8 \ \mu\text{m})$ polarimetric mapping by Weintraub et al. (1996) found the centroid of the polarization vectors to lie within 1" of the IRAS position; (ii) the discovery of radio continuum counterpart to IRAS 00338+6312 at 3.6 cm by Anglada et al. (1994), named "VLA 3", again within 1" of IRAS coordinates; (iii) additionally, Henning et al. (1992) detected a H₂O maser associated with IRAS 00338+6312. The above clearly indicated that FU Oris (RNO 1B/1C) are not physically associated with the outflow activity/ IRAS 00338+6312, but a deeply embedded YSO at the core of L1287 is energizing the source.

The second object of the present study, IRAS 03595+5110 is a strong far infrared source with its spectrum rising from 60 to 100 μ m. The IRAS PSC itself identified it with sources in 7 catalogues including AFGL, catalogues of: CO sources, H II regions and bright Galactic nebulae. The extended nature of IRAS 03595+5110 at mid and far infrared wavelengths led it to be included in the IRAS Small Scale Structure Catalog (X0359+511). This source is well inside the nebulosity of Sharpless source S 206, an evolved H II region, which has been studied extensively in optical and radio wavelengths. The evolved nature of this source is also supported by the fact that although strong CO molecular line emission has been found (Snell, Dickman & Huang, 1990), no outflow activity was detected. The most outstanding feature about S 206 is its geometry: it is an example of a "blister" type of H II region, i.e. a dense molecular cloud being illuminated /heated/ionized by a star positioned outside the cloud itself. Our line of sight to S 206 is roughly normal to the shortest line joining the exciting star and the outer surface of the molecular cloud. The region around IRAS 03595+5110 has been an important target for the following studies : mapping in near infrared (Pismis & Mampaso 1991) and radio continuum (Albert et al. 1986, Balser et al. 1995); and H_2O maser search (Henning et al. 1992).

Although the two sources chosen for the present study are positionally located close to nebulosities, one of them, IRAS 03595+5110, is genuinely associated with the nebula (an example of a very evolved star forming region), and the other one, IRAS 00338+6312, accidentally happens to be near the line of sight to the FU Oris, but actually represents an extremely young star forming region.

2. Observations

The two Galactic star forming regions, viz, IRAS 00338+6312 and RAFGL 5111, have been observed using the two band far infrared (FIR) photometer system at the Cassegrain focus of the TIFR 100 cm (F/8) balloon borne telescope. The FIR telescope was flown from the TIFR Balloon Facility, Hyderabad, in central India (Latitude = 17°.47 N, Longitude = 78°.57 E), on November 12, 1995. Details of the telescope and the observational procedure are given by Ghosh et al. (1988). Only a brief description is presented here. The two FIR bands use a pair of 2 × 3 composite Silicon bolometer arrays cooled to 0.3 K by liquid ³He, which view identical part of the sky simultaneously. The field of view of each bolometer is 1'.6. The sky is chopped along the cross-elevation axis at 10 Hz with a throw of 4'.2. The two FIR wavebands are defined by a cooled beam splitter (restrahlen filter) and other filters. The normalised transmission curves for the two bands of the FIR photometer are shown in Fig. 1, which have been measured in the laboratory using a Michelson spectrometer with a Golay cell as the reference detector. The effective wavelengths for the two bands, for a λ^{-1} emissivity law and ~ 36 K temperature are, 143 μ m and 185 μ m. Saturn was observed for absolute flux calibration as well as determination of the instrumental Point Spread Function (PSF) including the effect of sky chopping.

The simultaneous mapping in the two FIR bands was carried out by raster scanning the telescope along the cross-elevation axis across the target source area under study. Whereas IRAS 00338+6312 was covered by three rasters, RAFGL 5111 was covered twice. The chopped FIR signals were gridded in a two dimensional sky matrix (elevation \times cross elevation), with a cell size of 0.3×0.3 . The observed signal matrix was deconvolved using an indigeneously developed procedure using the Maximum Entropy Method (MEM) similar to Gull and Daniell, 1978 (see Ghosh et al., 1988, for details). The FWHM sizes of the deconvolved maps of the point-like source (Saturn) are 1.6×1.9 and 1.6×1.8 in the 143 and 185 μ m bands respectively. For improving the offline absolute aspect determination of the telescope, a pre-selected star $(m_B < 8)$ in a "clean" field located within 30' of the target FIR source, was mapped using an optical photometer. The optical maps were also generated by using the same 2-D MEM deconvolution procedure as used for the FIR signals. The resulting absolute positions of the maps are good to $\sim 1'$. The positions of the stars detected by the optical photometer (during the raster scans across the FIR target source), are used to correct for any systematic shifts. This procedure leads to an absolute positional accuracy in the FIR maps, to about 0.5.

3. The HIRES processed IRAS maps

The IRAS survey data at all four bands (12, 25, 60 & 100 μ m) for the relevant regions of the sky corresponding to IRAS 00338+6312 and RAFGL 5111 were HIRES processed (Aumann, Fowler & Melnyk, 1990) at Infrared Processing and Analysis Center (Caltech).¹

¹IPAC is funded by NASA as part of the part of the IRAS extended mission program under contract to JPL.

These maps for both the programme sources have been used in the present study to quantify flux densities and angular sizes at the four IRAS bands. They have also been used for generating temperature and optical depth maps when the source is resolved.

4. Results

4.1. IRAS 00338+6312

An area of $22' \times 7'$ centred on IRAS 00338+6312 was mapped in the two FIR bands at 143 and 185 μ m. The deconvolved TIFR maps at these two bands are presented in Fig. 2. The dotted lines in these figures, mark the boundary of the region covered by the telescope bore-sight. However, the actual observations extend beyond this boundary due to : (i) the size of the detector arrays; (ii) the sky chopping; & (iii) the effective PSF size. As a result, the MEM deconvolved intensity maps extend $\sim \pm 6'$ beyond the marked boundary along each axis. The insets show the deconvolved intensity contours for the point-like source (Saturn). Since the 185 μ m map has higher dynamic range, the isophot contours are shown upto 2.5% of the peak intensity (809 Jy/sq. arcmin), while at 143 μ m the isophot contours have been displayed only upto 10% level of the peak intensity (368 Jy/sq. arcmin),

The HIRES processed maps at all the four IRAS bands, for the source IRAS 00338+6312 are shown in Fig. 3. The peak intensities in these 12, 25, 60 & 100 μ m maps correspond to 8.2, 82.8, 312 & 284 Jy/sq. arcmin respectively. Although the dynamic range in all these maps is much larger, for the purpose of comparison with TIFR maps, the isophots have been shown upto 1% level of respective peak intensities. The angular resolutions achieved in these maps (In-Scan × Cross-Scan) are 0!45 ×0!93, 0!47×0!72, 0!78×1!37 and 1!65× 2!05 at 12, 25, 60 and 100 μ m respectively.

The positions of the peaks corresponding to IRAS 00338+6312 in 143 & 185 μ m maps,

are shifted by 12" & 33" respectively with respect to the IRAS PSC coordinates. Considering the absolute positional accuracy of our maps ($\approx 30''$) and errors in the IRAS coordinates, they are consistent.

The results of numerical aperture photometry on the peaks in all six maps, are presented in Table 1. The flux densities extracted from the HIRES maps (within 5' dia circle) are 1.4, 1.1, 1.1 & 1.2 times the IRAS PSC values at 12, 25, 60 & 100 μ m bands respectively. Interestingly, the uncertainties in the flux densities from the HIRES maps have been determined to be 24%, 7%, 1% & 3% at the four bands respectively, which mainly originate from the definitions of the local background levels (leading to overestimation). In addition, considering that the HIRES flux densities represent slightly larger solid angle than the PSC, it may be concluded that the PSC and HIRES data are consistent and IRAS 00338+6312 is unresolved by IRAS at all 4 bands.

The IRAS 00338+6312 has been resolved in both 143 & 185 μ m bands, but with a morphological difference. Whereas in the 143 μ m map, the FWHM size clearly shows the extended structure, $(1'9 \pm 0'.1 \times 2'.0)$, compared to $1'.6 \times 1'.9$ for Saturn); at 185 μ m the extension is clearly visible only at lower contour levels of 10 % ($3'.0 \times 3'.1$, compared to $2'.5 \times 2'.8$ for Saturn) and 5 % ($3'.5 \times 3'.6$, compared to the $2'.8 \times 3'.2$ for Saturn). These angular dimensions contain information regarding the dust temperature distribution around IRAS 00338+6312. Interestingly, the extension is in a direction perpendicular to the molecular outflow direction or the extension seen in the radio continuum map.

Although IRAS 00338+6312 has been resolved in both 143 & 185 μ m bands, the structural information is rather limited for generating meaningful spatial distribution of colour temperature/optical depth. Instead, an attempt has been made to construct a radiative transfer model of this source, which is consistent with all available observational data. The flux densities from the present study along with other data available from the literature, have been compiled to generate the Spectral Energy Distribution (SED) for IRAS 00338+6312, to constrain the model (Section 5.2).

4.2. RAFGL 5111 (IRAS 03595+5110)

For RAFGL 5111 (IRAS 03595+5110), an area of $24' \times 11'$ around this source was mapped in the two FIR bands. The deconvolved TIFR maps for RAFGL 5111 at 143 & 185 μ m are presented in Figs. 4 (a) & (b) respectively. The isophots in both the maps have been displayed upto the 10% level of the respective peak intensities. The peak intensities are 142 Jy/sq. arcmin at 143 μ m band and 99.2 Jy/sq. arcmin at 185 μ m band.

IRAS 03595+5110 (RAFGL 5111) has been resolved very well in both the TIFR maps, and the neighbouring source IRAS 04004+5114 has also been detected very clearly in both the bands, with some structural details too.

The positions of the global peaks corresponding to IRAS 03595+5110 in our 143 & 185 μ m maps, are shifted with respect to the IRAS PSC coordinates by 0'3 and 0'5 respectively. Considering our absolute positional accuracy, they are consistent. However, the position of the fainter nearby source corresponding to IRAS 04004+5114, is quite different in 143 & 185 μ m maps from the IRAS PSC coordinates.

The HIRES processed IRAS maps (upto 1% level of the peak) for the corresponding region around IRAS 03595+5110 are shown in Figs. 4(c) – (f). The peak intensities in the HIRES maps are 9.66, 93.4, 237 and 130 Jy /sq. arcmin at 12, 25, 60 & 100 μ m bands respectively. The angular resolutions achieved in these maps are 0.45×1.05, 0.47×0.83, 0.85×1.28 and 1.77×2.30 at 12, 25, 60 and 100 μ m respectively. At least in the 12, 25 and 60 μ m maps, IRAS 03595+5110 is very well resolved and at 100 μ m there is some indication of extension. The nearby source IRAS 04004+5114 is also seen clearly in all the four bands (though at 100 μ m, appropriate levels of the contours need to be chosen, to be able to see the peak corresponding to IRAS 04004+5114, in the presence of the much stronger emission from IRAS 03595+5110).

The ratios of the integrated flux densities in a 5' diameter circular aperture around IRAS 03595+5110 in the HIRES maps, to the corresponding IRAS PSC values are 11.3, 5.4, > 3.2 and 1.8 at 12, 25, 60 & 100 μ m bands respectively. This quantifies the extended nature of this source in these bands. All the flux density and position details are given in Table 1.

Although the IRAS (HIRES) maps have much higher dynamic range, the angular resolution of TIFR maps are superior to the IRAS maps (at least at 60 & 100 μ m), due to the smaller and circular beams employed. Since the TIFR beams at both the FIR bands are identical and all the observations are simultaneous, this dataset is very sensitive to detect gradients in colour temperature and/or dust optical depth in this source. Hence, we have generated maps for the colour temperature as well as for the optical depth at 150 μ m, assuming a dust emissivity law of $\epsilon_{\lambda} \sim \lambda^{-1}$. These colour temperature and optical depth maps, have been generated, by using an interpolation table relating the ratio of signals detected for the two bands to the dust temperature for the assumed emissivity law.

Since the 143 and 185 μ m maps in general have different dynamic ranges, the colour temperature/optical depth maps have been generated only for that region around IRAS 03595+5110, where the intensities in each map are above corresponding prescribed thresholds. These thresholds reflect the achieved dynamic ranges in the respective maps (which are 5 & 10 at 143 & 185 μ m bands). In addition, to be very conservative regarding claiming structural information in the temperature/optical depth maps, further averaging (over 3×3 pixels) of both the intensity maps at 143 & 185 μ m, have been carried out before computing the temperature/optical depth. A region about 5' × 4' in size around IRAS 03595+5110 (RAFGL 5111) qualifies the above criteria. The resulting colour temperature map, T(143/185), is shown in Fig. 5 (a). The dust colour temperature distribution shows interesting structure with one major peak and an indication of a hotter region to the east of our map (~ 2' east of the intensity peak). The temperature ranges between 20 and 43 K. The hottest dust is systematically offset to the west (by ≈ 1.1), from the peak position of the intensity maps. Such offsets have been predicted by "blister" type models of H II regions, where the exciting star lies near the edge/outside the molecular cloud (Icke, Gatley, & Israel, 1980). Hence, our dust temperature map further supports the "blister" type geometry for RAFGL 5111, which has been suggested in the literature from radio continuum maps (Albert et al. 1986).

The dust optical depth map of the same region at 150 μ m, τ_{150} , (for assumed emissivity law of $\epsilon_{\lambda} \sim \lambda^{-1}$) is shown in Fig. 5 (b). The τ_{150} map shows a peak (2.6×10⁻³) towards the east of the intensity peak and a negative gradient terminating in a minimum (5.2×10⁻⁴) towards the west. The minimum value of τ_{150} positionally corresponds to the maximum of T(143/185).

Although the HIRES maps at 60 and 100 μ m have relatively poorer angular resolution compared to the TIFR far infrared maps, they have been used to generate the colour temperature, T(60/100), and optical depth (τ_{100}) maps (see Figs. 5(c) & (d)) for the same region as in Figs. 5(a) & (b) . The intensity maps at 60 & 100 μ m were averaged over 1'× 1' before computing T(60/100) and τ_{100} in a manner similar to that described by Ghosh et al. (1993) for an emissivity law of $\epsilon_{\lambda} \sim \lambda^{-1}$. The T(60/100) map shows one major peak (67 K), slightly to the west and two minor peaks (46 K) to the east ($\sim 2'$) of the intensity peak. It is interesting to compare the T(60/100) map with the T(143/185) map. Both are very similar morphologically. In both the maps, the hottest dust is positioned to the west of the intensity peak corresponding to IRAS 03595+5110. This westward offset is larger for the T(143/185) map. This is again consistent with the predictions for an H II region with "blister" type geometry (Icke, Gatley & Israel, 1980). In addition, a local enhancement in dust temperature is seen in both T(60/100) and T(143/185) maps at the same position (~ 2' east of IRAS 03595+5110). The τ_{100} map shows two peaks, one to the east (10^{-3}) and other to the west (1.2×10^{-3}) of IRAS 03595+5110. The region between these peaks, around the IRAS source position, show a uniform value of τ_{100} . The only peak in τ_{150} map coincides with the eastern peak of τ_{100} . The ratio "r" (τ_{150}/τ_{100}) for the peak position (after correcting for λ^{-1} emissivity) is ~ 3.9. The other (western) peak in τ_{100} map is coincident with the minimum in τ_{150} , with r being 1.5. In the intervening region, r takes up intermediate values. The above may not be surprising, since the IRAS and TIFR maps are probing dust at different temperatures. The spatial variation in r, along the east-west line through IRAS 03595+5110, could indicate temperature and/or density gradient as expected in "blister" type geometry in this source.

4.2.1. IRAS 04004+5114

In order to appreciate the structural details of the fainter source (neighbouring RAFGL 5111), i.e. IRAS 04004+5114, the relevant regions of the TIFR (143 & 185 μ m) as well as IRAS HIRES (60 & 100 μ m) maps have been displayed in Fig. 6. For generating these 143 & 185 μ m maps, the observed signals corresponding to the nearby stronger source (IRAS 03595+5110) have been "masked" (*i.e.* as if no measurements are available at those locations) before carrying out the MEM deconvolution. The contour levels in all the four maps have been chosen appropriately to highlight the morphology of IRAS 04004+5114. The peak intensities in 143, 185, 60 & 100 μ m bands are 34.3, 31.7, 22.7 and 23.8 Jy /sq. arcmin respectively. Whereas the TIFR maps are shown to 40% of the respective peaks due to limited dynamic range, the HIRES maps contain structural information upto 1% of the corresponding peaks. Most of the approximately east-west (P.A. $\approx 75^{\circ}$) extension seen

for IRAS 04004+5114 in the HIRES 60 & 100 μ m maps, could have been explained by the scan track of the IRAS focal plane (IRAS detectors are rectangular with longer side in the cross-scan direction). But, even in the TIFR maps at 143 & 185 μ m (with circular beams), this source is extended along a similar position angle.

Flux densities for IRAS 04004+5114 (in all 6 bands) correspond to an aperture of size 3', since it is close to the boundary of the TIFR maps (see Table 1). The ratios of the flux densities obtained from the HIRES maps to the IRAS PSC values, for IRAS 04004+5114, are 2.3, 1.7, 1.5 and 1.4 at 12, 25, 60 & 100 μ m. These ratios also indicate that the source is extended.

5. Discussion

5.1. Radiative Transfer Modelling

Before going into the individual details of the observations of IRAS 00338+6312 and the RAFGL 5111 regions, in this section we describe the modelling procedure that has been adopted to interpret the results obtained for each of these sources.

5.1.1. Procedure "A": Modelling continuum emission from dust and gas

The star forming region has been modelled as a spherically symmetric cloud powered by a centrally embedded source, which could either be a single or a cluster of ZAMS star/(s). A schematic diagram of the geometry of the model is presented in Fig. 7. The cloud is assumed to be immersed in an isotropic radiation field (typical Interstellar Radiation Field, ISRF) and the interstellar gas consists of only hydrogen. The gas and the dust follow the same radial density distribution law, but with the following difference – whereas the gas exists throughout the cloud (i.e. right from the stellar surface upto the outer boundary of the cloud, R_{max}) there is a natural lower limit to the inner boundary, R_{min} , for the dust distribution (i.e. a cavity in the dust cloud). This is because the dust grains are destroyed when exposed to excessive radiative heating. The gas to dust ratio, where they co-exist ($R_{min} < r < R_{max}$), is assumed to be constant. The position of the ionization front, R_{HII} , depends on the spectral shape and luminosity of the exciting source, as well as the density of the gas. The case, $R_{HII} < R_{min}$ is also possible, if either the star is not hot enough and/or the density of gas around the star is quite high.

Modelling a specific star forming region involves matching its predictions to: (i) the observed emergent spectral energy distribution (SED) due to thermal emission from dust; (ii) the radial profiles at various wavelengths; and (iii) the radio continuum emission from the gas component. The models are further constrained by the total luminosity of the embedded energy source/s (as determined by integrating the observed SED). For all the models the dust component is assumed to be composed of three most commonly accepted types : Graphite, Astronomical Silicate and Silicon Carbide (SiC). All physical properties of the grains, *viz.*, absorption and scattering efficiencies, have been taken from Draine & Lee (1984) and Laor & Draine (1993). The size distribution of the dust grains is assumed in accordance with Mathis, Rumpl & Nordsiek (1977), to be a power law, *viz.*, $n(a)da \sim a^{-m}da$, $a_{min} \leq a \leq a_{max}$ with m = 3.5. The lower and upper limits of the grain size distribution a_{min} (0.01 μ m) and a_{max} (0.25 μ m) have been taken from Mathis, Mezger & Panagia (1983). The ISRF has been taken from Mathis, Mezger & Panagia (1983), and has been held fixed for all model runs.

The following parameters are explored in order to get an acceptable fit to all the data : (i) the nature of the embedded source, which could either be a single ZAMS star or a cluster of ZAMS stars consistent with the Salpeter Initial Mass Function; (ii) radial density distribution law (only three power laws have been explored, viz., $n(r) \approx r^0, r^{-1}$ or r^{-2}); (iii) the relative abundances of the three constituent grain types; (iv) total radial optical depth due to the dust (inclusive of all constituents) at a selected wavelength (τ_{100} at 100 μ m); (v) the gas to dust ratio by mass (the predicted radio continuum emission is sensitive to this); (vi) geometric details like $R_{max} \& R_{min}$ (R_{min} will not violate radiative destruction of grains).

The interstellar cloud is divided into ≈ 100 radial grids. Near both the boundaries, these grids are logarithmically spaced (in rest of the cloud, a linear grid has been used). The frequency grid consists of 89 points covering the wavelength range 944 Å to 5000 μ m.

The radiative transport through the dust-gas cloud has been carried out by using a programme based on the code CSDUST3 (Egan, Leung & Spagna 1988). We have improvised this code by generalizing the boundary conditions leading to much better flexibility for modelling typical astrophysical sources. Although originally this code considered only the dust component, we have modified it to consider and treat the interstellar gas (only hydrogen) along with dust in a self consistent manner. With this modification, it has been possible to predict the radio continuum emission also, using a very simple approach. This scheme considers photo-ionization and recombination, along with absorption due to the grains. Whereas self-absorption of the radio emission within the cloud has been considered, the gas-dust coupling has been neglected. Further details of the procedure are given by Mookerjea & Ghosh (1998).

For preserving the energetics precisely and self-consistently, the total energy available for heating of the dust component, includes the following three components (all components being binned into the respectively relevant spectral grid elements) : (i) the star cluster/ZAMS stellar luminosity in photons below the Lyman limit ($\lambda > 912$ Å); (ii) a part of the Lyman continuum luminosity of the embedded star, ($\lambda < 912$ Å), directly absorbed by the dust; and (iii) a fraction of the same reprocessed by the gas. The last contribution, *viz.*, the reprocessed Lyman continuum photons, has been quantified by the prescription of Aller & Liller (1969) that each Lyman continuum photon emitted by the star ultimately leads to one Ly- α photon and one Balmer- α photon.

5.1.2. Procedure "B" : Modelling line emission from the gas

A sophisticated scheme of radiation transfer through the interstellar gas component has been used to explain the line emission from the gas. These include infrared nebular/ionic fine structure lines. This procedure considers several prominent elements in the gas phase of the cloud. In addition to photoionization and recombination, other physical processes like collisional excitation & de-excitation, grain photoionization and gas-dust coupling are also included. This detailed modelling involves the use of the photoionization code CLOUDY (Ferland, 1996), which has been supplemented with a software scheme developed by Mookerjea & Ghosh (1998), to make the model predictions more realistic and easy to compare with observations. This scheme improves the modelling by (i) emulating the exact structure of the H II region; and (ii) including the absorption effects of the dust (present within the line emitting zones), on the emergent line intensities. It predicts physical conditions of the gas, e.g. ionization, level populations, temperature structure, and the emerging emission line spectrum. The gas component of the cloud has been considered with typical H II region abundance, as tabulated by Ferland (1996). Only the elements with abundance relative to hydrogen, higher than 3.0×10^{-6} have been used; these are – H, He, C, N, O, Ne, Mg, Si, S and Ar. The grains of the Astronomical Silicate and Graphite types have been introduced at and beyond a radial distance from the exciting star such that they do not heat up above their sublimation temperature.

The entire cloud is considered to be consisting of two spherical shells, the inner one made of gas alone and the outer one with gas and dust. The boundary between the two shells, R_{min} , is taken from the corresponding best fit model using Procedure "A". CLOUDY is run

twice, the first time (RUN1) for the inner pure gas shell with the central energy source. The resulting emergent continuum from RUN1 is used as input to the second run (RUN2) for the outer shell. The emerging line spectrum from RUN1 is transported to an outside observer, through the second (outer) shell by considering the extinction due to the entire dust column present there. For every spectral line considered, its emissivities from individual radial zones of RUN2 are transported through the corresponding remaining dust column densities within the outer shell. The emerging line luminosities from RUN1 and RUN2 are finally added to predict the total observable luminosity.

A total of 27 most prominent spectral lines (from various ionization stages of the above mentioned 10 elements) in the wavelength range $2.5 - 200 \ \mu$ m have been considered. From observational point of view, the reliable detectability of any spectral line will depend on experimental detail like : the instrumental line profile (spectral resolution); as well as the strength of the continuum in the immediate spectral neighbourhood of the line.

5.2. IRAS 00338+6312

This source has been modelled using Procedure "A" only, since no high resolution spectroscopic observation is available. We present here the model, which was found to be the most consistent with all available observations. The SED for IRAS 00338+6312 has been constructed from flux densities at the 4 IRAS bands (from HIRES maps) and the 2 TIFR bands. The flux densities at the sub mm wavelengths of 800 and 1100 μ m have been taken from JCMT observations by McCutcheon et al. (1995). The near-IR data (Persi et al. 1988; Weintraub & Kastner 1993) have not been used in the SED, since now it is clear that the RNO 1B/1C are not physically associated with IRAS 00338+6312.

The total color corrected luminosity of IRAS 00338+6312 as quoted by Wouterloot &

Brand (1989) is $3 \times 10^3 L_{\odot}$ for a distance of 1.61 kpc. However more recent observations give the distance to the source to be 1.1 kpc, implying the total luminosity to be ~ 1056 L_{\odot} (McCutcheon et al. 1995). The latter number has been used by us for modelling purposes. Snell, Dickman & Huang (1990) and Carpenter, Snell & Schloerb (1990) have determined the cloud mass from their CO measurements, to be between $2.2 \times 10^3 M_{\odot}$ (M_{LTE}) and 2.7×10^3 M_{\odot} (M_{virial}). Although the radio continuum observations of IRAS 00338+6312 by Carpenter, Snell & Schloerb (1990) and McCutcheon et al. (1991) at 6 cm failed detection, Anglada et al. (1994) successfully detected it at 3.6 cm (0.49 mJy). This radio continuum measurement has been used to fine tune the gas to dust ratio in the model for this source. The resulting best fit model is presented in Fig. 8. Although the fit obtained is quite good at the infrared wavelengths from 12 to 185 μ m, at the sub-mm wavelengths (800 & 1100 μ m) the model predicts a large excess over the observed fluxes. One possible explanation of this discrepancy is that, whereas the region mapped by JCMT does not cover the entire cloud, our model prediction displayed in Fig. 8 is the integrated emission from the entire cloud. The radius of the map shown by McCutcheon et al. (1995) is less than 0.3 pc, while other CO observations give the radius of the source to be $\sim 1.5~{\rm pc.}$ Our model predicts an outer radius of 1.1 pc. We have estimated the total flux densities at 800 and 1100 μ m by calculating the fraction of the total flux emitted from the area mapped by McCutcheon et al., from the model and corrected the observed fluxes accordingly. These extrapolated flux densities are quite close to the model predictions. The best fit model parameters are summarised in Table 2. The most surprising result from our modelling is that, the dust is radially distributed uniformly $(n_d \sim r^0)$. The models with density distribution as r^{-1} and r^{-2} yield extremely poor and unacceptable fits to the observed SED. The embedded energy source is a single ZAMS B2.5 type star. The inner dust radius (cavity size) is consistent with the dust sublimation at the relevant local radiation field. The role of external boundary condition in the form of assumed ISRF, is evident at wavelengths shorter than $\approx 3 \ \mu m$ in the SED. At these wavelengths, the backscattered ISRF dominates over the thermal dust emission. The total cloud mass corresponding to this model is $2.4 \times 10^3 M_{\odot}$, which is in excellent agreement with the mass determined from the CO data ($2.2 - 2.7 \times 10^3 M_{\odot}$; Carpenter, Snell & Schloerb, 1990). The expected angular sizes of IRAS 00338+6312 in the HIRES and TIFR maps have been estimated from the model, by convolving the predicted source size (at a particular wavelength band) with the achieved angular resolution (post image processing) in that band. These predictions are consistent with the sizes seen at 12, 25, 60, 100, 143 & 185 μ m maps.

Hence, our model for IRAS 00338+6312 can be called very successful since it not only fits the observed infrared sub-mm SED, but also selfconsistently explains the radio continuum emission and is consistent with the implications of the CO data.

5.3. RAFGL 5111 (IRAS 03595+5110)

Compared to the previous source (IRAS 00338+6312), modelling of RAFGL 5111 is rather involved, since it has a complex geometry as implied by its structure at widely different wavebands encompassing optical, infrared and radio wavelengths. IRAS 03595+5110 is associated with an evolved H II region with an optical nebula, S 206. This nebula appears to be open or mass-limited in the eastern direction and photon limited to the west (Deharveng, Israel & Maucherat 1976). The geometry is similar to the "blister" type of H II region, discussed by Icke, Gatley & Israel (1980), where a dense interstellar cloud is heated by a young star situated just outside the cloud (or near the boundary of the cloud). The position of IRAS 03595+5110 is situated near the centroid of the dense cloud, thereby representing the thermal mid & far infrared emission from the dust component. The distance to this source is 3.3 kpc (Snell, Dickman & Huang 1990). The exciting star (outside the cloud), has been identified to be BD $+50^{0}$ 886. This star of spectral type O6, can explain the energetics of IRAS 03595+5110, despite the geometrical dilution arising due to its far

location with respect to the cloud. The corresponding ionized nebula has been studied well at radio continuum as well as radio recombination lines. The VLA map at 20 cm by Albert et al. (1986) shows structure such that a 1-D cut in the east-west direction turns out to be consistent with the "blister" type model with an exciting star with luminosity $\approx 8.2 \times 10^4$ L_{\odot} , and $N_{Lyc} \approx 5.3 \times 10^{48}$ s⁻¹. The detailed study of this source at 3.4 cm by Balser et al. (1995) using interferometric (VLA; 8" beam) as well as single dish (100-m Effelsberg; 84" beam) measurements, has led to determination of many parameters. The single dish map has been modelled for a homogeneous spherical shell geometry as well as a spherical gaussian geometry. In either case, an O6.5 ZAMS exciting star is implied and the electron density, n_e , ranges between $180 - 240 \text{ cm}^{-3}$. However, the compact component resolved in the VLA map, when modelled, led to an O9.5 type of exciting star and $n_e \approx 770 \text{ cm}^{-3}$. The CO line emission has been detected from this source (Snell, Dickman & Huang 1990), but no outflow activity has been found. Searches for H_2O masers in the neighbourhood of this source have been unsuccessful. The above two points are consistent with the fact that in IRAS 03595+5110, one is dealing with a very evolved H II region/star forming region. The nebular ionic lines ([O III] at 52 & 88 μ m; [N III] at 57 μ m) in the far infrared have been detected from this source by Rubin et al. (1988).

The observed SED for IRAS 03595+5110 has been compiled from the following measurements : IRAS HIRES maps (12, 25, 60 & 100 μ m); TIFR maps (143 & 185 μ m) and RAFGL data (11, 20 & 27 μ m). The near-IR data of Pismis & Mampaso (1991) has not been used, since none of their peaks (IRS1/IRS2/IRS3) coincide with the IRAS source, which is not surprising. In fact their IRS1 is the exciting star BD +50⁰886.

In spite of the complex geometry of IRAS 03595+5110, we have attempted to construct a self consistent picture of this source using an "equivalent" spherically symmetric model. The artificial aspect in this "equivalent" model approach is that, an embedded energy source is incorporated, although, in actual reality, the cloud is heated/ionized/illuminated from outside. However, the problem can be made energetically "equivalent" by quantifying the luminosity intercepted in the actual case and using that as the luminosity constraint on the embedded source. Since, spectroscopic measurements of ionic lines are available for IRAS 03595+5110, it has been modelled using both Procedures "A" and "B".

5.3.1. Results from Procedure "A"

The derived parameters corresponding to the best fit model from Procedure "A" are presented in Table 2. This model corresponds to a uniform the dust density distribution $(n(r) \sim r^0)$. The embedded energy source is a single ZAMS O6.5 star with 52% of its total luminosity deposited in the cloud $(7.7 \times 10^4 L_{\odot})$. This special situation is demanded by the simultaneous fitting of the SED as well as the radio continuum emission. The model fit to the SED is shown in Fig. 8. The total radio continuum emission predicted by this model is 1.5 Jy at 8.75 GHz, which falls in between the values obtained from interferometric and single dish observations (Balser et al. 1995). The model predicts the electron density inside the H II region, n_e , to be 530 cm⁻³, which is again within the range of values obtained by Balser et al. (1995) from the VLA (770 cm⁻³) and single dish data (240 cm⁻³). The cloud mass from the CO observations (Snell, Dickman & Huang 1990) of the central 2' (dia) turns out to be $\approx 69 M_{\odot}$, which is similar to the mass of the central 2' of the model cloud, 46 M_{\odot} . Considering the complex geometry of IRAS 03595+5110, the above model can be called quite satisfactory.

5.3.2. Results from Procedure "B"

The modelling for IRAS 03595+5110 using the Procedure "B", has been carried out using the physical sizes and other parameters from the best fit model under scheme "A". In all 18 nebular/ionic lines satisfied our detectability criterion (which is the following : the power in the line is at least 1% of the power in neighbouring continuum for a resolution element determined by $R = \lambda/\Delta\lambda = 1000$). The wavelengths and luminosities of these lines are presented in Table 3. The complete emerging spectrum predicted by this model, including all lines from the 10 elements considered and the continuum, is shown in Fig. 9.

A comparison of observed line ratios, *viz.*, [O III (52 μ m)] / [O III (88 μ m)] and [N III (57 μ m)] / [O III (52 μ m)] (Rubin et al. 1988), with our model predictions are shown in Table 4. Whereas the former ratio is overestimated in the model, the latter is quite close to the measurements. The model predictions can be much better tested if this source is studied in many other infrared lines, by present/future space missions (ISO, SOFIA, SIRTF).

It is interesting to note that the mid to far infrared continuum levels predicted from the best fit models for RAFGL 5111 by Procedures "A" and "B" match within 20 - 30%. This is remarkable, considering the diverse approaches of the two procedures.

5.4. IRAS 04004+5114

This faint source in the neighbourhood of RAFGL 5111, which was also mapped at the two TIFR bands, has been considered for radiative transfer modelling using Procedure "A". Its observed SED has been constructed from the IRAS HIRES data (at 12, 25, 60 & 100 μ m) and the TIFR data (at 143 & 185 μ m). The distance to IRAS 04004+5114 has been taken to be 2.6 kpc (Wouterloot, Brand & Fiegle 1993).

The spherically symmetric dust cloud model fitting the observed SED best, corresponds

to : a constant density cloud (i.e. $n(r) \sim r^0$); an embedded star of type A3 with total luminosity $1.7 \times 10^3 L_{\odot}$. Other derived parameters are listed in Table 2. The model fit to the SED for IRAS 04004+5114 is shown in Fig. 8. It can be seen that the model fits the available observations very well. The predicted radio emission for this source is 0.1 mJy at 5 GHz.

6. Summary

Two Galactic star forming regions associated with the IRAS sources 00338+6312 and 03595+5110 (RAFGL 5111) have been studied in detail. The source IRAS 00338+6312, is very controversial since earlier it was thought to be excited by FU Orionis type activity, though only recently evidences showed that it is a very young and deeply embedded object in a much earlier evolutionary phase of star formation. The second source is associated with an evolved H II region in a molecular cloud (S 206), excited by a star located outside the cloud itself (an example of "blister" type geometry). Although both these sources have red nebular objects in their IRAS error ellipses, they represent probably two extremes in stage of evolution of star forming regions.

Both these sources have been mapped (angular resolution ~ 1.5) simultaneously in two far infrared bands ($\lambda_{\text{eff}} = 143 \& 185 \ \mu\text{m}$), using the TIFR 100 cm balloon borne telescope. The HIRES processed IRAS survey data for the same region at 12, 25, 60 & 100 μ mhave also been used for comparison.

Whereas IRAS 00338+6312 is only slightly extended (and hence resolved only in the TIFR maps), IRAS 03595+5110 is well resolved in both the TIFR bands, as also in some IRAS bands. The faint source in the neighbourhood of RAFGL 5111, *viz.*, IRAS 04004+5114, has also been resolved in the TIFR bands. The dust colour temperature, T(143/185), and

optical depth, τ_{150} , maps have been generated for RAFGL 5111. Similarly the T(60/100), and τ_{100} maps have been generated from IRAS data for comparison. These maps show interesting structures implying dust density and/or temperature gradient along a line joining the external exciting star and the outer boundary of the cloud.

Two independent radiative transfer modelling procedures have been implemented in spherical geometry, for a dust-gas cloud with an embedded energy source at the centre. The observed SED, radio continuum data, infrared fine structure line strengths etc. have been used to optimise these models. The resulting models for IRAS 00338+6312, 03595+5110 and 04004+5114 have been presented. The most important conclusion is that for all the above three sources, the best fit models correspond to the uniform radial density distribution law $(n(r) \sim r^0)$. Intuitively one would expect a centrally peaked radial density distribution in star forming regions. Identical conclusion has been found in the studies of several similar Galactic star forming regions (Faison et al. 1998, Campbell et al. 1995, Colome et al. 1995, Butner et al. 1994; Mookerjea & Ghosh 1998). The model predictions of nebular line intensities for RAFGL 5111, are in reasonable agreement with observations.

Acknowledgements

We would like to thank IPAC (Caltech) for providing the HIRES processed IRAS data. Gary Ferland is thanked for his help on many occasions regarding the code CLOUDY. It is a pleasure to thank S L D'Costa, M V Naik, D M Patkar, M B Naik, S A Chalke, S V Gollapudi, G S Meshram and C B Bakalkar of the Infrared Astronomy Group for their technical support to the Far Infrared Astronomy Programme. Thanks are due to M N Joshi, S Sreenivasan, J V Subbarao and other colleagues of TIFR Balloon Facility at Hyderabad for smoothly conducting the balloon flight and related operations. We also thank all members of the Control Instrumentation (CIBA) Group.

We thank the anonymous referee and Steven Willner (Scientific Editor) for their sug-

gestions which improved the presentation of the paper.

REFERENCES

- Albert C.E., Schwartz P.R., Bowers P.F. & Rickard L.J. AJ, 92, 75, 1986.
- Aller L.H. & Liller W., Stars and Stellar Systems, Vol. VII, 500, 1969.
- Anglada G., Rodriguez L.F., Girart J.M., Estalella R. & Torrelles J.M. ApJ, 420, L91, 1994.
- Aumann H.H., Fowler J.W. & Melnyk M. AJ, 99, 1674, 1990.
- Balser D.S., Bania T.M., Rood R.T. & Wilson T.L. ApJS, 100, 371, 1995.
- Butner H.M., Evans N.J., Lester D. F., Levreault R. M. & Strom S.E. ApJ, 420, 326, 1994.
- Campbell M.F., Butner H.M., Harvey P.M., Evans N.J., Campbell M.B. & Sabbey C.N. ApJ, 454, 831, 1995.
- Carpenter J.M., Snell R.L. & Schloerb F.P. ApJ, 362, 147, 1990.
- Colome C., Harvey P.M., Lester D.F., Campbell M.F. & Butner H.M. ApJ, 447, 236, 1995.
- Deharveng L., Israel F.P. & Maucherat M. A&A, 48, 63, 1976.
- Draine B.T. & Lee H.M., ApJ, 285, 89, 1984.
- Egan M.P., Leung C.M., Spagna G.F., Computer Physics Communications, 48, 271, 1988.
- Faison M., Churchwell E., Hofner P., Hackwell J., Lynch D.K. & Russell R.W. ApJ, 500, 280, 1998.
- Ferland G.J., Hazy, a Brief Introduction to CLOUDY, Univ. of Kentucky, Dept. of Phys. and Astron. Internal Reports, 1996.
- Ghosh S.K., Rengarajan T.N., Verma R.P. & Karnik A.D. "Interplay between Massive Star Formation, the ISM and Galaxy Evolution", Proc. of 11th IAP Astrophysics Meeting, 499-500 (1996).

- Ghosh S.K., Iyengar K.V.K, Rengarajan T.N., Tandon S.N., Verma R.P. & Daniel R.R. ApJ, 330, 928, 1988.
- Ghosh S.K., Verma R.P., Rengarajan T.N., Das B. & Saraiya H.T. ApJS, 86, 401, 1993.
- Gull S.F. & Daniell G.J. Nature, 272, 686, 1978.
- Henning T., Cesaroni R., Walmsley M. & Pfau W. A&AS, 93, 525, 1992.
- Icke V., Gatley I. & Israel F.P. ApJ, 236, 808, 1980.
- Karnik A.D., Ghosh S.K., Rengarajan T.N., Tandon S.N. & Verma R.P. Bull. Astron. Soc. India, in press, 1999.
- Kenyon S.J., Hartmann L., Gomez M., Carr J.S. & Tokunaga A. AJ, 105, 1505, 1993.
- Laor A. & Draine B.T., ApJ, 402, 441, 1993.
- Mathis J.S., Mezger P. G., Panagia N. A & A, 128, 212, 1983.
- Mathis J.S., Rumpl W., Nordsiek K.H. ApJ, 217, 425, 1977.
- McCutcheon W.H., Dewdney P.E., Purton R. & Sato T. AJ, 101, 1435, 1991.
- McCutcheon W.H., Sato T., Purton C.R., Matthews H.E. & Dewdney P.E. AJ, 110, 1762, 1995.
- McMuldroch S., Blake G.A. & Sargent A.I. AJ, 110, 354, 1995.
- Mookerjea B. & Ghosh S.K. (submitted), 1998.
- Mookerjea B., Ghosh S.K., Karnik, A.D., Rengarajan T.N., Tandon S.N. & Verma R.P. Bull. Astron. Soc. India, *in press*, 1999.

- Persi P., Ferrari-Toniolo M., Busso M., Robberto M., Scaltriti F. & Silvestro G. AJ, 95, 1167, 1988.
- Pismis P. & Mampaso A. MNRAS, 249, 385, 1991.
- Rubin R.H., Simpson J.P., Erickson E.F. & Haas M.R. ApJ, 327, 377, 1988.
- Snell R.L., Dickman R.L. & Huang Y.-L. ApJ, 352, 139, 1990.
- Staude H.J. & Neckel Th. A&A, 244, L13, 1991.
- Verma R.P., Rengarajan T.N. & Ghosh, S.K. Bull. Astron. Soc. India, 21, 489, 1993.
- Weintraub D.A. & Kastner J.H. ApJ, 411, 767, 1993.
- Weintraub D.A., Kastner J.H., Gatley I. & Merrill K.M. ApJ, 468, L45, 1996.
- Wouterloot J.G.A. & Brand J. A&AS, 80, 149, 1989.
- Wouterloot J.G.A, Brand J. & Fiegle K. A&AS, 98, 589, 1993.

This manuscript was prepared with the AAS ${\rm IAT}_{\rm E}\!{\rm X}$ macros v4.0.

Fig. 1.— Normalized spectral responses of the two far infrared bands of the TIFR photometer system. The solid line corresponds to the band with $\lambda_{eff} = 143 \ \mu m$ and the dashed line corresponds to the band with $\lambda_{eff} = 185 \ \mu m$.

Fig. 2.— TIFR Intensity maps for IRAS 00338+6312 : (a) at 143 μ m the Peak = 368.0 Jy/sq. arcmin ; Contour levels = 10, 20, 30, 40, 50, 60, 70, 80, 90, 95% of the peak; (b) at 185 μ m the Peak = 809.0 Jy/sq. arcmin ; Contour levels = 2.5, 5.0, 10, 20, 30, 40, 50, 60, 70, 80, 90, 95% of the peak. The insets show deconvolved images of Saturn in the respective bands. The contours are 50, 70 and 90 % of respective peaks, aligned to the instrumental axes for meaningful comparison. "+" shows the IRAS PSC position of the source.

Fig. 3.— HIRES processed IRAS maps of IRAS 00338+6312: (a) at 12 μ m, (b) 25 μ m, (c) 60 μ m and (d) 100 μ m with peaks = 8.2, 82.8, 312 and 284 Jy/sq. arcmin respectively. The contour levels are 1, 2.5, 5, 10, 20, 30, 40, 50, 60, 70, 80, 90 & 95 % of the peaks in corresponding bands.

Fig. 4.— (a) & (b) show TIFR maps for IRAS 03595+5110 at 143 μ m, (Peak = 142.0 Jy/sq. arcmin) and at 185 μ m (Peak = 99.2 Jy/sq. arcmin) respectively. The contour levels are the same as in Fig. 2(a). The insets are identical to those in Fig. 2. "+" shows the IRAS PSC position of the source. (c), (d), (e) & (f) show HIRES processed IRAS maps of the same source at 12 μ m, 25 μ m, 60 μ m and 100 μ m with peaks = 9.66, 93.4, 237 and 130 Jy/sq. arcmin respectively. The contour levels are the same as in Fig. 3.

Fig. 5.— (a) & (c) show the T(143/185) and T(60/100) maps respectively of the source IRAS 03595+5110. The contours in (a) are at 20, 22, 24, 25, 27, 30, 32, 35, 40 & 43 K. The contours in (c) are at 24, 25, 26, 28, 33, 37, 42, 51, 55, 60, 64, 67 K. (b) & (d) show the τ_{150} and τ_{100} maps repectively. The peak in (b) is 2.7×10^{-3} and the contours shown are the same fractions of the peak as in Fig. 2(b). The peak in (d) is 1.25×10^{-3} and the contours are same fractions of the peak as in Fig. 2(a). "+" shows the IRAS PSC position of the source. All the maps have been generated assuming $\epsilon_{\lambda} \sim \lambda^{-1}$ emissivity law.

Fig. 6.— (a) & (b) show specially processed (see text) TIFR maps for IRAS 04004+5114 at 143 μ m (Peak = 34.3 Jy/sq. arcmin) and 185 μ m (Peak = 31.7 Jy/sq. arcmin) respectively. Contour levels = 40, 60,80, 100% of the respective peaks. The "+" shows the IRAS PSC position of the source. (c) & (d) show HIRES maps of the same source, at 60 μ m (Peak = 22.7 Jy/sq. arcmin) and 100 μ m (Peak = 23.8 Jy/sq. arcmin) respectively. The contour levels are the same as in Fig.3

Fig. 7.— Schematic diagram of the interstellar cloud with an embedded star.

Fig. 8.— Spectral energy distributions for IRAS 00338+6312, IRAS 04004+5114 and IRAS 03595+5110. For all the sources the continuous line represents the best fit radiation transfer model (procedure "A") and the points represent observations. For better visibility the SEDs of IRAS 04004+5114 and IRAS 03595+5110 have been shifted by -4 and -9 dex respectively.

Fig. 9.— Emergent spectrum from model calculations of IRAS 03595+5110, using procedure "B".

Table 1. Positions (143 μm or 185 $\mu m)$ and flux densities of the sources from TIFR and IRAS HIRES maps.

Source	Posi	$F_{12\mu m}$	$F_{25\mu m}$	$\mathrm{F}_{60\mu\mathrm{m}}$	$F_{100\mu m}$	$F_{143\mu m}$	$F_{185\mu m}$	
	R.A. (1950)	Dec. (1950)	Jy	Jy	Jy	Jy	Jy	Jy
00338+6312 (5 ' dia)	00 ^h 33 ^m 53. ^s 3	+63°12′32″	2.5	22.4	389	829	1615	2317
03595+5110 (5 ' dia)	03 ^h 59 ^m 31. ^s 6	+51°10′41″	58.6	314.7	1462	1405	883	829
04004+5114 (3 ' dia)	04 ^h 00 ^m 26. ^s 1	+51°14′45″	6.4	11.3	72	146	100	118

Table 2. Best fit parameters for the three sources modelled, using Procedure "A".

Source	R _{max} (pc)	$ m R_{min}$ (pc)	$ au_{100}$	Luminosity $(10^3 L_{\odot})$	Silicate : Graphite	N_e (cm^{-3})	${ m M}_{ m Dust}$ (M_{\odot})	Gas:Dust
00338+6312	1.1	0.0001	0.15	1.8	31.9:68.1	1.8×10^{4}	47.2	50:1
03595 + 5110	5.0	0.002	0.0095	77.0	98.3:1.7	530	65.22	100:1
04004+5114	0.25	0.0003	0.08	1.7	21.4:78.6	8.4×10^{4}	129.2	100:1

Element &	Wavelength	Luminosity	
Ionization stage	(µm)	(L_{\odot})	
C II	157.74	15.03	
ΟΙ	145.6	0.12	
N I	121.8	1.15	
O III	88.42	75.25	
ΟΙ	63.23	2.02	
N III	57.26	35.50	
O III	51.85	161.50	
Ne III	36.04	4.75	
Si II	34.84	4.10	
S III	33.50	73.00	
O IV	25.91	0.57	
Ar III	21.84	1.69	
S III	18.69	66.75	
Ne III	15.57	50.75	
Ne II	12.82	15.43	
S IV	10.52	23.48	
Ar III	8.99	19.99	
Ar II	7.00	1.57	

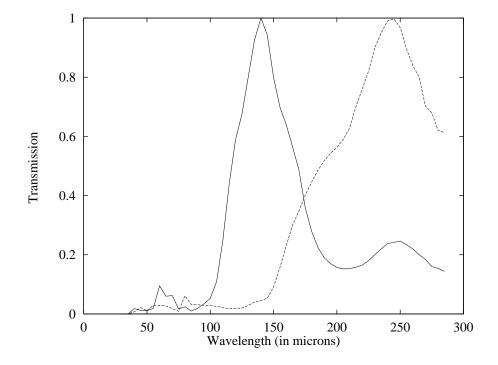
Table 3. Emergent line luminosities predicted by the model for IRAS 03595+5110, using Procedure "B".

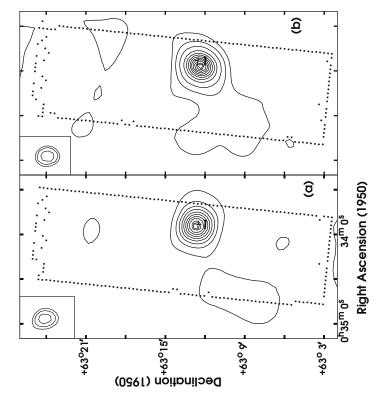
- 34 -

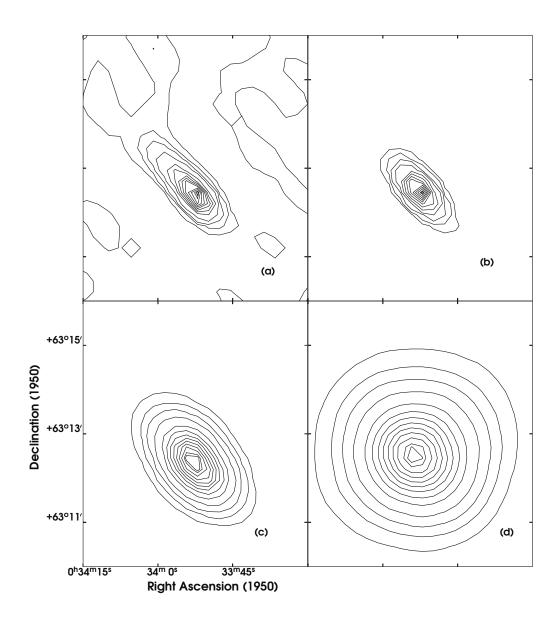
Table 4. Comparison of model predictions of line ratios with observations.

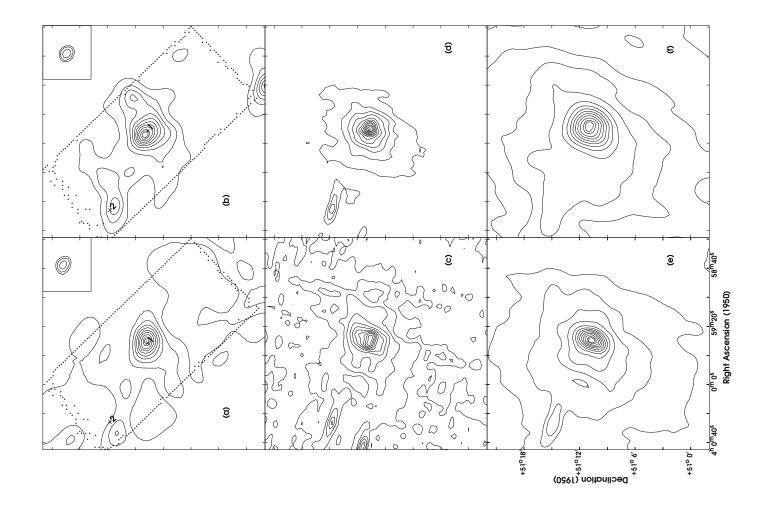
Lines	Observations ^a	Model (Procedure "B")
$[{\rm O~III}~(52\mu{\rm m})]~/~[{\rm O~III}~(88\mu{\rm m})]$	1.38 ± 0.07	2.15
[NIII (57µm)]/ $[$ OIII (52µm)]	0.18 ± 0.013	0.22

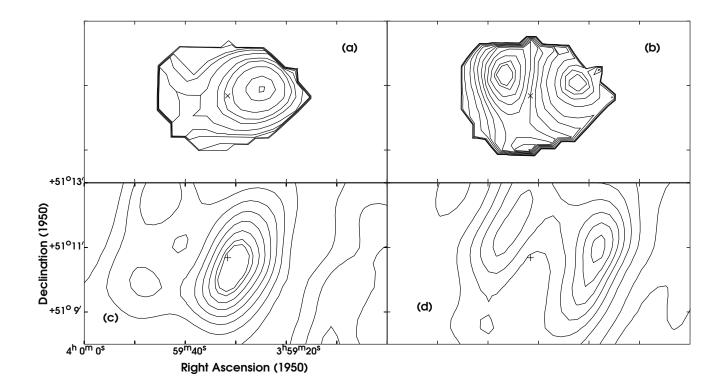
^aRubin et al. (1988)

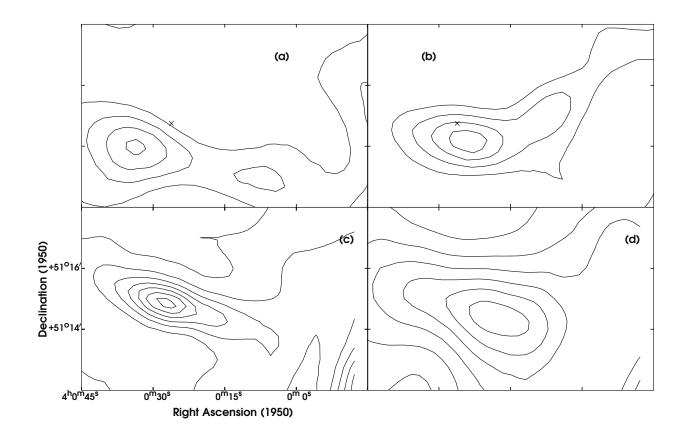












1 ··· · · · ·

